BBA - General Subjects xxx (xxxx) xxx–xxx

Contents lists available at ScienceDirect

BBA - General Subjects

journal homepage: www.elsevier.com/locate/bbagen

# An insight into the dependence of the deamination rate of human APOBEC3F on the length of single-stranded DNA, which is affected by the concentrations of APOBEC3F and single-stranded DNA

Li Wan[a,b], Keisuke Kamba[a], Takashi Nagata[a,b,*], Masato Katahira[a,b,*]

[a] Institute of Advanced Energy, Kyoto University, Gokasho, Uji, Kyoto, Japan
[b] Graduate School of Energy Science, Kyoto University, Gokasho, Uji, Kyoto, Japan

ARTICLE INFO

*Keywords:*
Real-time NMR
APOBEC3F
Deamination
ssDNA
Activity

ABSTRACT

*Background:* APOBEC3F (A3F), a member of the human APOBEC3 (A3) family of cytidine deaminases, acts as an anti-HIV-1 factor by deaminating deoxycytidine in the complementary DNA of the viral genome. A full understanding of the deamination behavior of A3F awaits further investigation.

*Methods:* The real-time NMR method and uracil-DNA glycosylase assay were used to track the activities of the C-terminal domain (CTD) of A3F at different concentrations of A3F-CTD and ssDNA. The steady-state fluorescence anisotropy measurement was used to examine the binding between A3F-CTD and ssDNA with different lengths. The use of the A3F-CTD N214H mutant, having higher activity than the wild-type, facilitated the tracking of the reactions.

*Results:* A3F-CTD was found to efficiently deaminate the target deoxycytidine in long ssDNA in lower ssDNA concentration conditions ([A3F-CTD] ≫ [ssDNA]), while the target deoxycytidine in short ssDNA is deaminated efficiently in higher ssDNA concentration conditions ([A3F-CTD] ≪ [ssDNA]). This property is quite different from that of the previously studied A3 family member, A3B; the concentrations of the proteins and ssDNA had no effect.

*Conclusions:* The concentrations of A3F-CTD and ssDNA substrates affect the ssDNA-length-dependence of deamination rate of the A3F-CTD. This unique property of A3F is rationally interpreted on the basis of its binding characteristics with ssDNA.

*General significance:* The discovery of the unique property of A3F regarding the deamination rate deepens the understanding of its counteraction against HIV-1. Our strategy is applicable to investigate the other aspects of the A3 activities, such as those involved in the cancer development.

## 1. Introduction

On human chromosome 22, there is a cluster of genes encoding the APOBEC3 (A3) family of polynucleotide cytidine deaminases [1]. All members of the A3 family deaminate deoxycytidines into deoxyuridines on single-stranded DNAs (ssDNAs) synthesized from retroviral genomic RNAs and endogenous retrotransposons [2,3]. Therefore, A3 family members are regarded as part of the innate immune system [4,5]. Additionally, some of the A3 family members were implicated as a chronic cause of DNA damage in cancers such as cervical, bladder, and breast ones [6–8].

The A3 family comprises seven members, APOBEC3A (A3A), APOBEC3B (A3B), APOBEC3C (A3C), APOBEC3D (A3D), APOBEC3F (A3F), APOBEC3G (A3G), and APOBEC3H (A3H). They have either one (A3A, A3C, and A3H) or two deaminase domains (A3B, A3D, A3F, and A3G). The single deaminase domains are catalytically active, while of the double ones, only the C-terminal domains (CTDs) are catalytically active [9]. These catalytic deaminase domains share the consensus zinc (Zn)-binding motif, histidine (His)-X-glutamic acid (Glu)-$X_{23–28}$-proline (Pro)-cysteine (Cys)-$X_{2–4}$-cysteine (Cys), where X can be any amino acid; the His and two Cys residues, as well as a water molecule, coordinate with $Zn^{2+}$ to form a tetrahedral complex [1,9–11]. The acid/base catalytic Glu residue converts the water molecule into a nucleophilic hydroxide ion, which attacks the 4th position of the cytosine nucleobase. Subsequently, a transient tetrahedral intermediate is formed and the 4-$NH_2$ group is eliminated as ammonia, resulting in the formation of a uracil nucleobase [12–14].

Among the A3 family members, A3C, A3D, A3F, A3G, and A3H were

* Corresponding authors at: Institute of Advanced Energy, Kyoto University, Gokasho, Uji, Kyoto, Japan.
*E-mail addresses:* nagata.takashi.6w@kyoto-u.ac.jp (T. Nagata), katahira@iae.kyoto-u.ac.jp (M. Katahira).

https://doi.org/10.1016/j.bbagen.2019.04.011
Received 30 January 2019; Received in revised form 20 March 2019; Accepted 8 April 2019

found to restrict the replication of human immunodeficiency virus 1 (HIV-1) that is deficient in a viral countermeasure, i.e., a viral infectivity factor (Vif) [15]. A3G, which has the highest deamination rate, targets 5′-CCC-3′ (the underlined deoxycytidine is primarily deaminated), while 5′-TC-3′ is targeted by the other six A3 family members including A3F [16–20]. Importantly, A3G and A3F have been regarded as primary and secondary HIV-1 restrictors, respectively, according to their high antiviral activity among the members [21–24]. In the absence of Vif, A3F and A3G are packaged into HIV-1 virions via incorporation/encapsidation, and then, during reverse transcription in the newly infected cell, they convert deoxycytidines to deoxyuridines in viral minus-strand DNA [25–27]. This C-to-U conversion promotes G-to-A hypermutation of the HIV-1 genome, as well as a decrease in the accumulation of HIV-1 reverse transcripts. The latter is catalyzed by cellular enzymes; uracil-DNA glycosylases excise the uracils in the HIV-1 reverse transcripts, and subsequently the resulting abasic-sites are cleaved by endonucleases [28]. However, HIV-1 has the above-mentioned accessory protein, Vif, by which HIV-1 neutralizes the effects of A3F and A3G activity; Vif hijacks the cellular Cullin5 E3 ubiquitin ligase, directly binds to A3F and A3G, and recruits them for proteasomal degradation through ubiquitination [25,29,30]. Therefore, the development of drugs that disrupt the binding of Vif with A3F and A3G have been attractive in the field of pharmaceutical research. On the other hand, several studies have revealed that, depending on the cellular context, the range of mutagenesis by A3 family members can vary greatly, some are lethal to HIV-1 but some are not. This is problematic since it may induce sublethal HIV-1 mutations that fuel viral heterogeneity and immune escape [31–35]. In this regard, knowledge concerning the characteristics of the deamination rate of the A3 family members is thought to be important.

The research on A3F was focused mostly on its interaction with Vif [36–39]. Later on, biochemical analysis of A3F regarding deamination rate has attracted increasing attention due to its biological significance, as well as to prevent the sublethal HIV-1 mutagenesis mentioned above. Recently, the roles of ssDNA-binding and the deamination rate of the amino acid residues located in the loops surrounding the catalytic center of A3F has been determined by using a combination of functional mutagenesis, steady-state fluorescence anisotropy measurement, and uracil-DNA glycosylase (UDG) assaying [40].

Previously, we applied the real-time NMR method to investigate the characteristics of the deamination rate and enzymatic action of A3G-CTD [41–45] and A3B-CTD [46]. We analyzed the data by constructing either a kinetic or mathematical model [42,46]. For A3G-CTD, we revealed a location- and sequence-dependent deamination mechanism, the nucleic acid determinants of the preferred targets, and the salt and pH dependences of the deaminase reaction [43–45]. Here, we report the ssDNA length-dependent deamination rate of A3F-CTD, and the effect of concentrations of A3F-CTD and ssDNA investigated by the real-time NMR method and UDG assaying. We found that the ssDNA length-dependence of the deamination rate of A3F-CTD is affected by the concentrations of A3F-CTD and ssDNA in the system. The dependence turned out to be quite different from that of A3B-CTD. We rationally interpreted the dependence on the ssDNA length and effect of the concentrations on the deamination rate of A3F-CTD, based on the ssDNA-binding characteristics of A3F-CTD.

## 2. Materials and methods

### 2.1. Plasmids and ssDNA substrates

A DNA fragment encoding the wild-type (WT) A3F-CTD (187–373) was inserted into the *Nde*I/ *Eco*RI sites of the pET28b (+) plasmid. The expression plasmid for the A3F-CTD N214H mutant was constructed by oligonucleotide-directed PCR mutagenesis, following the manufacturer's procedure for a KOD-Plus-mutagenesis kit (TOYOBO, Japan) [40]. All the plasmids were confirmed by DNA sequencing before transfer into BL21 (DE3) Gold. The fluorescein isothiocyanate (FITC)-labeled ssDNA substrates and unlabeled ssDNA substrates used for real-time NMR experiments, which were obtained from FASMAC Co., Ltd. (Japan), are listed in Table 1.

**Table 1**
List of ssDNA oligonucleotides used in this study.

| Name | Sequence[a] |
|---|---|
| $S_{FITC\_10}$ | 5′-(FITC) ATATTCAAAG-3′ |
| $S_{FITC\_49}$ | 5′-(FITC) ATAATAATAA TAATAATAAT AATATTCATT TATAATAATA ATAATAATA-3′ |
| $S_{10}$ | 5′-AAATTCAAAG-3′ |
| $S_{46}$ | 5′-AAAAAAAAAA AAAAAAAAAA ATTCAAAAAA AAAAAAAAAA AAAAAA-3′ |

[a] The 5′-TC-3′ sequence containing the target cytosine is underlined.

### 2.2. Preparation of the proteins

The recombinant WT A3F-CTD and N214H mutant, each containing an N-terminal hexahistidine tag, were expressed in BL21 (DE3) Gold. The procedures for protein expression and purification were described previously [40].

### 2.3. Deamination rate assay

Measurement of in vitro deamination rate was performed using the UDG assay as described previously [40,46]. Briefly, 1 μM protein was mixed with 100 nM FITC-labeled ssDNA substrate in 15 mM Tris-HCl (pH 7.5), containing 50 mM NaCl and 5 mM DTT. The 10 nt ($S_{FITC\_10}$) and 49 nt ($S_{FITC\_49}$) ssDNAs were used as substrates. The reaction solution was incubated at 37 °C for 1 h. The reaction was quenched by heating at 95 °C for 5 min. Subsequently, two units of uracil DNA glycosylase (UDG, New England Biolabs) was added to the solution, which was then incubated at 37 °C. After 1 h, this solution was heated under alkaline conditions. The deamination products were detected by electrophoresis on a 20% denaturing polyacrylamide gel. The gel was scanned with a Pharos FX™ Molecular Imager (BIO-RAD) and analyzed using Quantity One 1D analysis software (BIO-RAD). The deamination percentage was calculated by dividing the intensity of the product by the total intensity of the product and un-reacted substrate. Error bars represent the standard deviation for three independent experiments.

### 2.4. Real-time NMR spectroscopy

The NMR reaction solutions were prepared by dissolving ssDNA in 15 mM Tris-HCl (pH 7.5), containing 50 mM NaCl and 5 mM DTT. The final concentration of ssDNA was adjusted to 150 μM. The 10 nt ($S_{10}$) and 46 nt ($S_{46}$) ssDNAs were used as substrates. NMR spectra were recorded at 25 °C with a Bruker AVANCE III 600, which was equipped with a *Z*-axis gradient cryoprobe (Bruker Biospin). After addition of the WT A3F-CTD or N214H mutant at the final concentration of 1 μM to the NMR reaction solution, a series of two-dimensional TOtal Correlated SpectroscopY (2D TOCSY) spectra with a mixing time of 20 ms were recorded. The signal intensities of the H5-H6 correlation peaks of the target cytosines were quantified using SPARKY [47]. The intensity of the peak of cytosine obtained at each time point was individually fitted to a single exponential decaying function, $I(t) = I_s \exp.(-kt) + I_b$, where $I_b$ is the baseline intensity of the spectrum, $I_s + I_b$ the intensity of the correlation peak of each deoxycytidine at time point zero, and $k$ the apparent deamination rate constant [43–45]. The error bars were obtained by nonlinear least-squares analysis [48].

### 2.5. Steady-state fluorescence anisotropy assay

Examination of the binding between the N214H mutant and ssDNAs

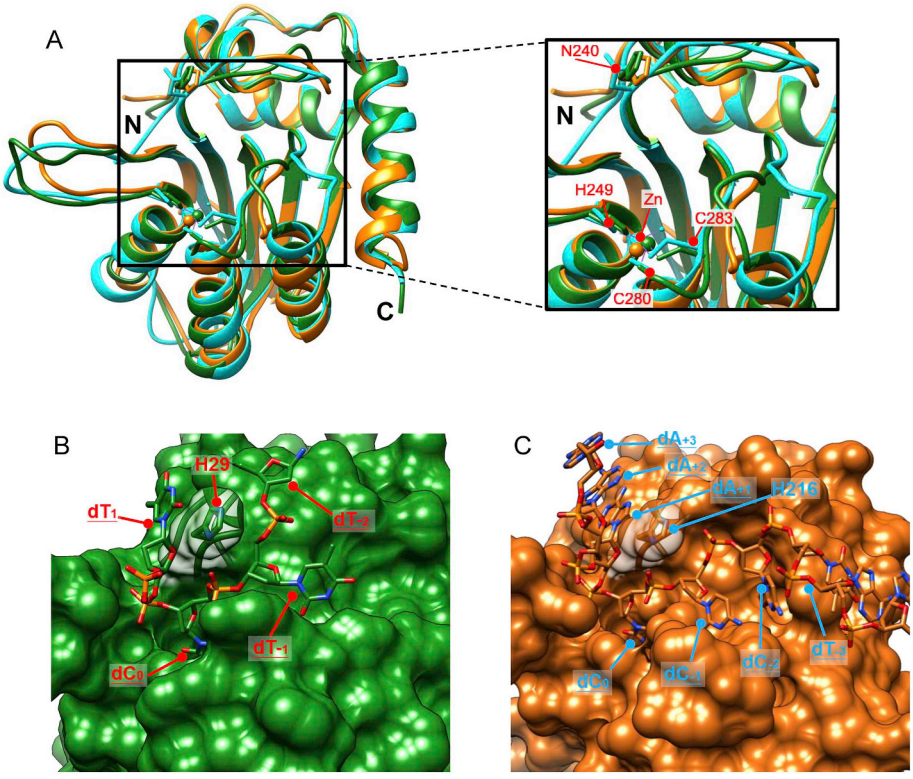


**Fig. 1.** Structure comparison of A3F-CTD, A3A, and A3G-CTD. (**A**) Superposition of the structures of A3F-CTD in the free form (PDB: 3WUS, cyan), and A3A (PDB: 5SWW, green) and A3G-CTD (PDB: 6BUX, orange), each in a complex with ssDNA. The side chains of N214 of A3F-CTD, H216 of A3G-CTD, and H29 of A3A are shown as sticks. The $Zn^{2+}$ ions are shown as balls and the side chains of the $Zn^{2+}$ coordinating residues are indicated by sticks. (**B**) Surface presentation of A3A in the complex. The transparency of the surface at H29 is 60%. The side chain of H29 and the 5'-TTCT-3′ moiety of ssDNA are indicated by sticks. (**C**) Surface presentation of A3G-CTD in the complex. The transparency of the surface at H216 is 60%. The side chain of H216 and the 5'-AATCCCAAA-3′ moiety of ssDNA are indicated by sticks. The orientation of the structures in (B) and (C) is the same as in (A). The nitrogen, oxygen, phosphorus, and sulfur atoms are colored blue, red, orange, and yellow, respectively. (For interpretation of the references to color in this figure legend, the reader is referred to the web version of this article.)

was conducted by means of the steady-state fluorescence anisotropy (FA) assay [40]. Here, 100 nM of either $S_{FITC\_10}$ or $S_{FITC\_49}$ was titrated with small aliquots of the N214H mutant at 25 °C. The concentrations of the N214H mutant during the titration ranged from 0 to 1.5 μM. The dissociation constant values ($K_d$) were obtained by fitting FA data using the following equations.

(i) Binding between N214H and $S_{FITC\_10}$ [46].

The chemical equation for binding of N214H and $S_{FITC\_10}$ can be written as follows:

$$DNA + A3F \rightleftarrows DNA - A3F$$

where N214H and $S_{FITC\_10}$ are expressed as A3F and DNA, respectively.

The FA value, fl(obs), can be expressed as follows:

$$fl(obs) = fl(complex)\bullet\frac{[DNA - A3F]}{[DNA(total)]} + fl(free)\bullet\frac{[DNA(total)] - [DNA - A3F]}{[DNA(total)]} \quad (1)$$

where fl(free) and fl(complex) are the FA values for free DNA and the DNA − A3F complex, respectively. "[ ]" are the concentrations of the molecules. [DNA(total)] indicates the concentration of the total DNA in the solution.

$$[DNA - A3F] = \frac{[DNA(total)] + [A3F(total)] + K_d - \sqrt{(([DNA(total)] + [A3F(total)] + K_d)^2 - 4\bullet[DNA(total)]\bullet[A3F(total)])}}{2}$$

where [A3F(total)] indicates the total concentration of A3F added to the solution.

The curve-fitting of FA data was performed using Microsoft Excel.

(ii) Binding between N214H and $S_{FITC\_49}$ [23,40].

We denote N214H and $S_{FITC\_49}$ as A3F and DNA, respectively. Since, the binding curve obtained on FA assaying was a sigmoidal curve, we used the Hill equation to model cooperative binding. The chemical equation for binding can be written as follows:

$$DNA + h\bullet A3F \rightleftarrows DNA - h\bullet A3F.$$

The following equation can be derived from the Hill equation:

$$\frac{[DNA - h\bullet A3F]}{[DNA(total)]} = \frac{[A3F]^h}{[A3F]^h + {K_d}^h}$$

where $h$ is a Hill coefficient, and under the current conditions, $h > 1$. [DNA(total)] indicates the total concentration of DNA in the solution. Therefore, the FA value, fl(obs), can be expressed as follows:

$$fl(obs) = fl(complex)\bullet\frac{[A3F]^h}{[A3F]^h + {K_d}^h} + fl(free)\bullet\frac{{K_d}^h}{[A3F]^h + {K_d}^h}$$

where fl(free) and fl(complex) are the FA values for free DNA and the DNA − h·A3F complex, respectively.

The curve-fitting of FA data was performed using GraphPad Prism 7 using the following equation:

$$fl(obs) \simeq fl(complex)\bullet\frac{[A3F(total)]^h}{[A3F(total)]^h + {K_d}^h} + fl(free)\bullet\frac{{K_d}^h}{[A3F(total)]^h + {K_d}^h} \quad (2)$$

where [A3F(total)] indicates the total concentration of A3F added to the solution.

## 3. Results and discussion

### *3.1. The A3F-CTD N214H mutant has higher deamination rate than the wild-type*

Previously, we showed that the deamination rate of A3F-CTD increases substantially on substitution of a histidine for N214, and we named the mutant N214H [40]. We also showed that this N214H mutation confers pH dependence to the deamination rate of A3F-CTD.

Since, the N214H mutant exhibits the highest activity around pH 5.5, we thought the protonation of the histidine results in a positive effect on the ssDNA binding and the deamination rate [40]. The corresponding residues in well studied A3A and A3G are H29 and H216, respectively (Fig. 1A). In both of these proteins, it has been shown that this histidine plays an important role in the pH dependent substrate binding and deamination rate [49,50]. Very recently, the co-crystal structures of A3A with a ssDNA containing 5′-TCT-3′ and A3G with a ssDNA containing 5′-CCCA-3′ indicated that the histidine makes many contacts with the ssDNA (the target deoxycytidines are underlined and are named the "0" position, $dC_0$) [51,52]. H29 of A3A undergoes π-π interactions with the +1 position dT ($dT_1$), and forms hydrogen bonds with the 5′ phosphate groups of $dT_{-1}$, $dC_0$, and $dT_1$ (Fig. 1B). Similarly, H216 of A3G undergoes π-π interactions with the +1 position dA ($dA_1$), and forms hydrogen bonds with the 5′ phosphate groups of $dC_{-1}$ and $dC_0$ (Fig. 1C). These structures revealed that the many contacts of the histidine with the nucleotides proximal to $dC_0$ support proper positioning of $dC_0$ as to the catalytic center. This is also likely the case with the N214H mutant of A3F-CTD.

We applied the real-time NMR method to measure the deamination rate of both N214H mutant and WT A3F-CTD, against 10 nucleotides oligonucleotide $S_{10}$, which contains the target deoxycytidine at the sixth position ($dC_6$) (Table 1) (Fig. 2A). The time course of the change in intensity of the H5-H6 TOCSY correlation peak of the $dC_6$ in the $S_{10}$ ssDNA was monitored (Fig. 2B and C). As shown in Fig. 2C, > 80% of the $dC_6$ in the $S_{10}$ ssDNA was deaminated within 23 h by the N214H mutant, while in the case of the WT A3F-CTD, only about 20% of the $dC_6$ in the $S_{10}$ ssDNA was deaminated even after 45 h. The apparent deamination rate of the N214H mutant was nearly 10-fold higher than that of WT (Fig. 2C). This finding clearly indicates that the N214H mutant has higher deamination rate than the WT A3F-CTD, which is consistant with our previous results obtained on uracil DNA glycosylase (UDG) assaying [40].

Next, to determine whether or not the WT A3F-CTD and N214H mutant show length-dependence in their deamination rate, we carried out a UDG assay (Fig. 3). Two ssDNA substrates with lengths of 10 nt ($S_{FITC\_10}$, Table 1) and 49 nt ($S_{FITC\_49}$, Table 1) were used as representative short and long substrates, respectively. Both the $S_{FITC\_10}$ and $S_{FITC\_49}$ substrates contain a single 5′-TC-3′ target sequence located near the center, which are the sixth ($dC_6$) and twenty-seventh ($dC_{27}$) positions, respectively. The concentration of the $S_{FITC\_10}$ and $S_{FITC\_49}$ substrates was 0.1 μM, while that of the WT A3F-CTD and N214H mutant was 1 μM. Fig. 3C shows that both the WT A3F-CTD and N214H mutant deaminated the target deoxycytidine in the $S_{FITC\_49}$ substrate much more efficiently than the one in the $S_{FITC\_10}$ substrate. Thus, we confirmed that the N214H mutant retains the same length-dependent deamination rate as the WT A3F-CTD, and therefore we decided to use the N214H mutant for further analysis using the real-time NMR method.

### 3.2. The concentrations of the ssDNA substrate and A3F-CTD affect the ssDNA-length-dependent deamination rate of A3F-CTD

To determine whether or not the concentrations of A3F and the substrate ssDNA have an effect on the ssDNA-length-dependence of the deamination rate of A3F, the real-time NMR method was performed for the N214H mutant with a ssDNA concentration higher than that of the N214H mutant; 150 μM 10 nt and 46 nt ssDNA ($S_{10}$ and $S_{46}$, Table 1), which are representative short and long ssDNAs, respectively, and 1 μM N214H mutant were used. Thus, here, the situation is [N214H] ≪ [ssDNA]. Both the $S_{10}$ and $S_{46}$ ssDNAs contain a single 5′-TC-3′ target sequence located near the center, which are the sixth ($dC_6$) and twenty-fourth ($dC_{24}$) positions, respectively. In the case of the UDG assay, the concentrations of N214H and ssDNAs were 1 μM and 0.1 μM, respectively, that is, [N214H] ≫ [ssDNA]. The intensities of the H5-H6 TOCSY correlation peaks of the target $dC_6$ and $dC_{24}$ for the $S_{10}$ and $S_{46}$ ssDNAs, respectively, were plotted for each ssDNA against time points (Fig. 4A). The intensity of the $dC_6$ in the $S_{10}$ ssDNA decreased significantly faster than that of the $dC_{24}$ in the $S_{46}$ one. The apparent deamination rate of the N214H mutant was about 2.5-fold higher toward the $S_{10}$ ($0.076 \pm 0.005\ h^{-1}$) than toward the $S_{46}$ ($0.037 \pm 0.005\ h^{-1}$) (Fig. 4B), indicating that the N214H mutant deaminates the target deoxycytidine in 10 nt ssDNA more efficiently. This finding is opposite to the result obtained with the UDG assay, in which the N214H mutant deaminated the target deoxycytidine in 49 nt ssDNA more efficiently (about 1.5-fold more efficiently) (Fig. 3C). Therefore, investigation of the effect of the concentrations of ssDNA and the N214H mutant on the ssDNA-length-dependent deamination

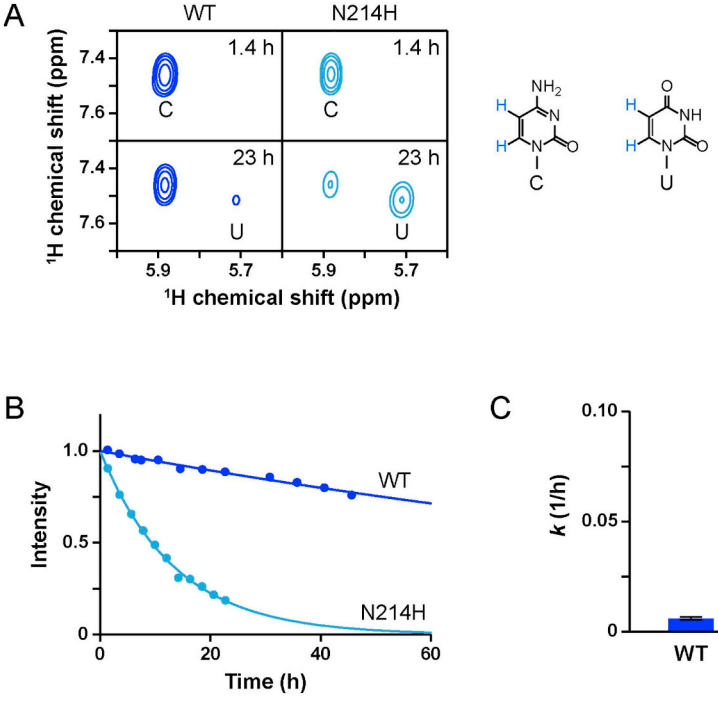


**Fig. 2.** Deaminase activities of WT and N214H mutant A3F-CTDs measured by real-time NMR. Either WT or N214H mutant A3F-CTD was added to the substrate ssDNA, containing a target deoxycytidine. (**A**) A region of the 2D TOCSY spectrum for the H5–H6 correlation peaks of deoxycytidine and deoxyuridine of 10 nt ssDNA, $S_{10}$, at the 1.4 h and 23 h time points after addition of either WT or N214H mutant A3F-CTD. (**B**) Time courses of the relative intensities of the target deoxycytidine in 10 nt $S_{10}$ catalyzed by WT (blue) and N214H mutant (cyan) A3F-CTDs. (**C**) The apparent deamination rate constants for WT and N214H mutant A3F-CTDs toward 10 nt $S_{10}$ are shown; the reactions were carried out with the concentrations of 1 μM protein and 150 μM ssDNA. (For interpretation of the references to color in this figure legend, the reader is referred to the web version of this article.)

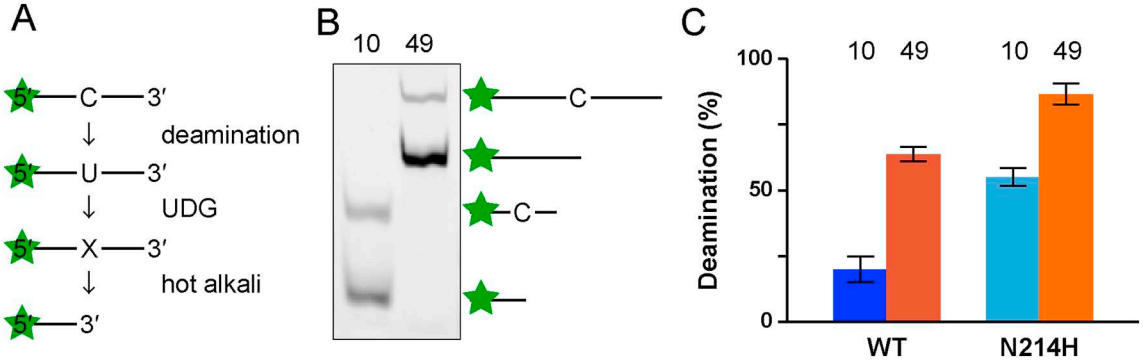


**Fig. 3.** Measurement of the deamination rate of WT and N214H mutant A3F-CTDs toward ssDNAs of different lengths using the UDG assay. (**A**) Schematic diagram of the UDG assay. ssDNA, containing a target deoxycytidine at the center, was 5′-FITC labeled. (**B**) The deaminase activities of the N214H mutant toward 10 nt $S_{FITC\_10}$ and 49 nt $S_{FITC\_49}$ were examined. The bands are labeled on the right of the gel either as to the unreacted substrate or the deaminated product. (**C**) The percentages of the deamination products obtained on catalysis by WT and N214H mutant A3F-CTDs using $S_{FITC\_10}$ and $S_{FITC\_49}$ as substrates. The reactions were carried out with the concentrations of 1 μM protein and 0.1 μM ssDNA.

rate of the N214H mutant indicated that with a lower ssDNA concentration (UDG assay), the deamination reaction is efficient for long ssDNA, while it is efficient for short ssDNA with a higher ssDNA concentration (real-time NMR method). This is quite different from previously studied A3B. In the case of A3B, the deamination of the target deoxycytidine in short ssDNA (10 nt) is more efficient than that in long ssDNA (46 nt or 49 nt) both with low (0.1 μM) and high ssDNA (200 μM) concentrations, the concentration of A3B being 1 μM in both cases [46].

### 3.3. Examination of the binding of N214H to short and long ssDNAs

Next, we examined the ssDNA-binding affinity of the N214H mutant by means of the FA assay. 10 nt and 49 nt FITC-labeled ssDNA ($S_{FITC\_10}$ and $S_{FITC\_49}$, Table 1) were used as substrates. As shown in Fig. 5A and B, the FA values of both $S_{FITC\_10}$ and $S_{FITC\_49}$ increased upon the addition of the N214H mutant, indicating the formation of the N214H-ssDNA complex. The $K_d$ value of the binding between the N214H mutant and 10 nt ssDNA was obtained by fitting the binding curve (Fig. 5A) using Eq. (1), by which the value of $K_d$ = 0.43 μM was obtained (Table 2). In the case of the binding between the N214H mutant and 49 nt ssDNA, the binding curve (Fig. 5B) turned out to be a sigmoidal one, indicating the binding is positively cooperative. Therefore, we applied the Hill equation and used Eq. (2) to fit the binding curve, by which a Hill coefficient of 2.2 and a $K_d$ value of 0.85 μM were obtained (Table 2). These results suggest that two or more N214H molecules may cooperatively bind to the 49 nt ssDNA, while the 10 nt ssDNA is basically bound by one N214H molecule. Previously, Fang et al. showed the presence of transient interactions between two A3F-CTD molecules by using size exclusion chromatography at 4 °C [24]. Therefore, we suggest that the N214H molecules have some affinity to each other and in the presence of a ssDNA and only if the ssDNA is long enough, two or more N214H molecules can contact each other and undergo positively cooperative DNA-binding. We assume that the 49 nt ssDNA is long enough, while the 10 nt ssDNA is not.

### 3.4. Insights into the effect of the concentrations of the ssDNA substrate and A3F-CTD on the ssDNA-length-dependent deamination rate of A3F-CTD

Fig. 6 summarizes the effect of the concentrations of ssDNA and the N214H mutant on the ssDNA-length-dependent deamination rate of the N214H mutant.

For real-time NMR, 1 μM N214H and 150 μM either the short or long ssDNA substrate ($S_{10}$ or $S_{46}$), which fulfill the conditions of [N214H] ≪ [ssDNA], were used. Under these conditions, the efficiency of deamination by N214H was higher toward $S_{10}$ than toward $S_{46}$. The concentrations of N214H bound to $S_{10}$ and $S_{46}$ were calculated to be 0.997 μM and 0.994 μM, respectively, using the $K_d$ values obtained in the previous section. This indicates that nearly 100% of the N214H was bound to both $S_{10}$ and $S_{46}$. In the case of when $S_{10}$ was used as the substrate, N214H could effectively deaminate the target deoxycytidine, if N214H reached the target deoxycytidine from the landed position. On the other hand, in the case of when $S_{46}$ was used as the substrate, there is some probability of N214H landing to a region distant from the target deoxycytidine, because $S_{46}$ is longer than $S_{10}$. It was reported previously that A3F searches the target deoxycytidine by jumping [23]. This suggests that if N214H lands to the distant region of $S_{46}$, it needs to jump more times or farther to reach the deoxycytidine than when it lands on the $S_{10}$. In other words, N214H has more chance to dissociate while searching, and thereby cannot reach the target deoxycytidine for deamination, when it lands on the $S_{46}$. We propose this is the reason why 46 nt ssDNA is poorer substrate than the 10 nt ssDNA when [N214H] ≪ [ssDNA].

In the UDG assay, 1 μM N214H and 0.1 μM either the short or long

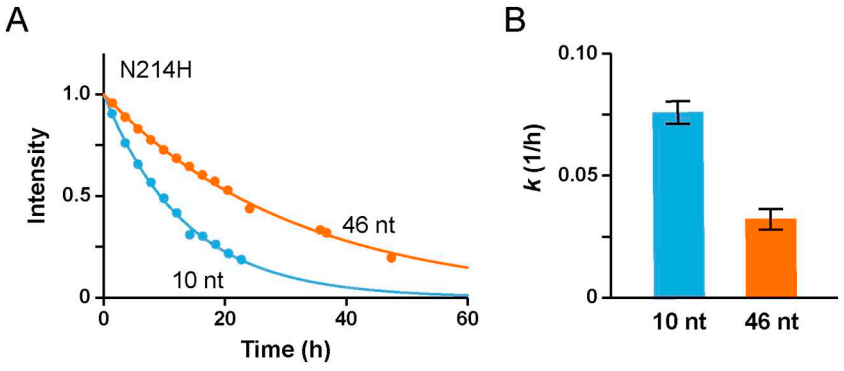


**Fig. 4.** Measurement of the deamination rate of the N214H mutant toward ssDNAs of different lengths using real-time NMR. (**A**) Time courses of the intensities of the target deoxycytidines in 10 nt $S_{10}$ (cyan) and 46 nt $S_{46}$ (orange). (**B**) The apparent deamination rate constants for the N214H mutant toward $S_{10}$ and $S_{46}$ are shown; the reactions were carried out with the concentrations of 1 μM protein and 150 μM ssDNA. (For interpretation of the references to color in this figure legend, the reader is referred to the web version of this article.)

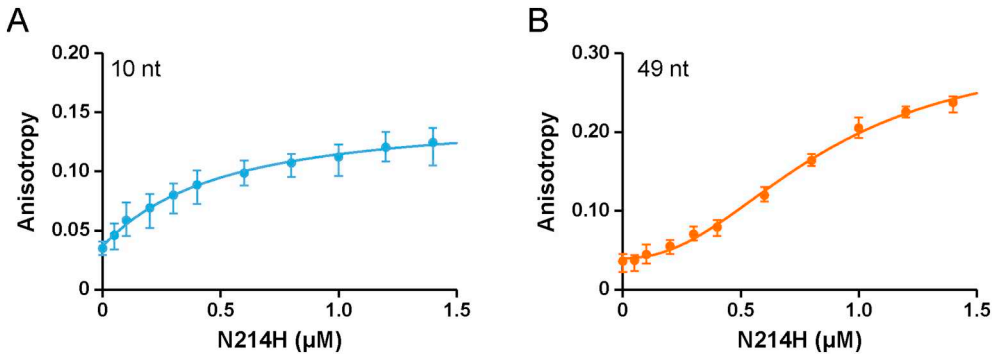


**Fig. 5.** The steady-state fluorescence anisotropy based-binding assaying of the N214H mutant with $S_{FITC\_10}$ and $S_{FITC\_49}$ (**A** and **B**). The data represent the averages of six individual measurements with error bars. The concentrations of $S_{10}$ and $S_{46}$ were 0.1 μM.

**Table 2**
ssDNA binding affinity and Hill constants of N214H.

| DNA length (nt) | 10 | 49 |
|---|---|---|
| $K_d$ (μM) | 0.43 ± 0.03 | 0.85 ± 0.10 |
| Hill constant | – | 2.2 ± 0.3 |

ssDNA substrate ($S_{FITC\_10}$ or $S_{FITC\_49}$), which fulfill the conditions of [N214H] ≫ [ssDNA], were used. Under these conditions, the efficiency of deamination by N214H was higher toward $S_{FITC\_49}$ than toward $S_{FITC\_10}$. By using the $K_d$ values obtained above, the concentrations of $S_{FITC\_10}$ and $S_{FITC\_49}$ that were bound by N214H were calculated to be 0.0683 μM and 0.0589 μM, respectively. Therefore, the concentration of N214H bound to $S_{FITC\_10}$ was calculated to be 0.0683 μM, while the concentration of N214H bound to $S_{FITC\_49}$ was deduced to be ca. 0.13 μM by taking the Hill constant of 2.2 into account in the latter case. In this situation, the amount of N214H bound to $S_{FITC\_49}$ was about 1.9-fold (0.13/0.0683≃1.9) higher than the amount of N214H bound to $S_{FITC\_10}$. In the current result, the efficiency of deamination by N214H was 1.5-fold higher toward $S_{FITC\_49}$ than toward $S_{FITC\_10}$ (Fig. 3C). To obtain this result, the required percentage of the N214H molecules that are bound to $S_{FITC\_49}$ and can reach the target deoxycytidine for deamination, α, is deduced to be 79% (1.9 × α/100 = 1.5, α = 79%). In other words, the experimental results under [N214H] ≫ [ssDNA] conditions can be rationally interpreted by assuming the α value of 79%. On the other hand, if we hypothesize only 50% of the N214H bound to $S_{FITC\_49}$ can reach the target deoxycytidine for deamination, the amount of N214H that can reach the target deoxycytidine for $S_{FITC\_49}$ is 0.95-fold (1.9 × 50/100 = 0.95) lower than that for $S_{FITC\_10}$. This cannot explain the experimental results, which indicates that the α value should not be 50%.

We have assumed in the previous section that the 49 nt ssDNA is long enough for N214H to carry out positive cooperative DNA-binding, while the 10 nt ssDNA is not. We also mentioned above that N214H that lands to the distant region of $S_{FITC\_49}$ needs to jump more times or farther to reach the deoxycytidine, and thereby may have higher chance to dissociate than N214H that lands on $S_{FITC\_10}$. We can conclude here that in the context of [N214H] ≫ [ssDNA], the amount of N214H that lands, and reaches and deaminates the target deoxycytidine on the $S_{FITC\_49}$ appears higher owing to the positive cooperative DNA-binding capability of N214H toward $S_{FITC\_49}$, although the amount of N214H that dissociates is more when it binds to $S_{FITC\_49}$.

The situation is quite different from A3F in the case of A3B. We previously reported that the deamination rate of A3B against the target deoxycytidine in short ssDNA is more efficient than that in long ssDNA both under low and high ssDNA concentrations [46]. The affinity of the

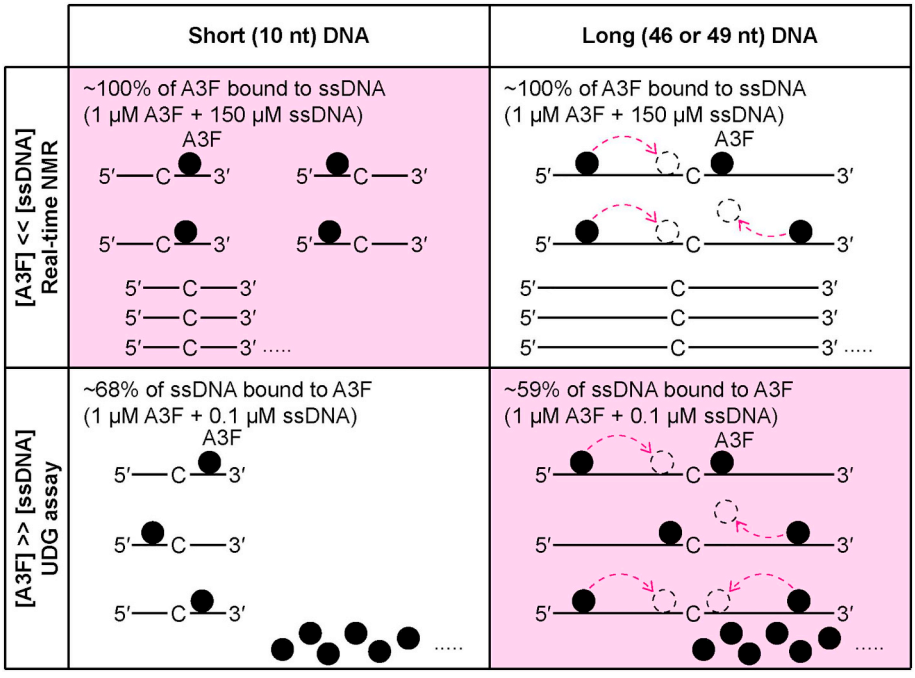


**Fig. 6.** The effect of the concentrations of A3F and ssDNA on the deamination rate of A3F, which is ssDNA-length-dependent. (Top) [N214H] ≪ [ssDNA] context (Real-time NMR conditions). The concentrations of N214H bound to $S_{10}$ and $S_{46}$ were calculated to be 0.997 μM and 0.994 μM, respectively, which are almost 100%. In this context, the target deoxycytidines on the 10 nt ssDNAs were efficiently deaminated (highlighted in pink) compared to those on the 46 nt ssDNAs. (Bottom) [N214H] ≫ [ssDNA] context (UDG assay conditions). The concentrations of $S_{FITC\_10}$ and $S_{FITC\_49}$ that were bound by N214H were calculated to be 0.0683 μM and 0.0589 μM, respectively. The concentrations of N214H bound to $S_{FITC\_10}$ and $S_{FITC\_49}$ were found to be 0.0683 μM and ca. 0.13 μM using the Hill constant (see details of calculation in the main text). In this context, the target deoxycytidines on the 49 nt ssDNAs were efficiently deaminated (highlighted in pink) compared to those for the 10 nt ssDNAs.

A3B toward the ssDNA is too low that the dissociation constant could not be obtained [46]. We therefore suppose that the A3B molecules do not undergo cooperative binding toward DNA. As a result, under the conditions of [A3B] ≫ [ssDNA] (that corresponds to the lower portions of Fig. 6), the concentration of A3B bound to long DNA (the lower right panel of Fig. 6) is not higher than that bound to short DNA (the lower left panel of Fig. 6). This is the reason why the dependence of the deamination rate of A3B on the length of ssDNA is not affected by the concentrations of A3B and ssDNA, i.e., short DNA is always deaminated more effectively than long DNA for A3B.

## 4. Conclusion

In this study, we investigated the effect of the concentrations of ssDNA substrates and A3F-CTD on the ssDNA-length-dependent deamination rate of the A3F-CTD. The use of the A3F-CTD N214H mutant, which exhibits higher deamination rate than the wild-type, allowed us to apply the real-time NMR method. In the context of the [A3F-CTD] ≫ [ssDNA] conditions, as observed with the UDG-assay, A3F-CTD showed higher deamination efficiency toward the target deoxycytidine in the long ssDNA substrate. However, in the context of the [A3F-CTD] ≪ [ssDNA] conditions, which was observed by real-time NMR method, the target deoxycytidine in the short ssDNA was deaminated more efficiently by A3F-CTD. These results were rationally interpreted by considering the binding characteristics of the A3F-CTD as to substrate ssDNAs of different lengths.

## Conflicts of interest

The authors declare no conflicts of interests.

## CRediT authorship contribution statement

**Li Wan:** Conceptualization, Data curation, Formal analysis, Investigation, Methodology, Validation, Visualization, Writing - original draft, Writing - review & editing. **Keisuke Kamba:** Formal analysis, Investigation, Methodology, Validation, Visualization, Writing - review & editing. **Takashi Nagata:** Conceptualization, Formal analysis, Funding acquisition, Investigation, Methodology, Project administration, Resources, Software, Supervision, Validation, Visualization, Writing - original draft, Writing - review & editing. **Masato Katahira:** Conceptualization, Formal analysis, Funding acquisition, Investigation, Methodology, Project administration, Resources, Software, Supervision, Validation, Writing - review & editing.

## Acknowledgements

This work was supported by JSPS KAKENHI to M. K. (Nos. 18H04550 and 18K19397) and T.N. (Nos. 17H05878 and 17K07307). We thank Professors T. Morii and E. Nakata of Kyoto University for their technical support with the fluorescence gel imaging systems.

## References

[1] A. Jarmuz, A. Chester, J. Bayliss, J. Gisbourne, I. Dunham, J. Scott, N. Navaratnam, An anthropoid-specific locus of orphan C to U RNA-editing enzymes on chromosome 22, Genomics 79 (3) (2002) 285–296.
[2] S.G. Conticello, The AID/APOBEC family of nucleic acid mutators, Genome Biol. 9 (6) (2008) 229.
[3] R.C. Beale, S.K. Petersen-Mahrt, I.N. Watt, R.S. Harris, C. Rada, M.S. Neuberger, Comparison of the differential context-dependence of DNA deamination by APOBEC enzymes: correlation with mutation spectra in vivo, J. Mol. Biol. 337 (3) (2004) 585–596.
[4] A. Koito, T. Ikeda, Intrinsic immunity against retrotransposons by APOBEC cytidine deaminases, Front. Microbiol. 4 (2013) 28.
[5] N.K. Duggal, M. Emerman, Evolutionary conflicts between viruses and restriction factors shape immunity, Nat. Rev. Immunol. 12 (10) (2012) 687–695.
[6] K.J. Kuong, L.A. Loeb, APOBEC3B mutagenesis in cancer, Nat. Genet. 45 (9) (2013) 964–965.
[7] P. Pham, A. Landolph, C. Mendez, N. Li, M.F. Goodman, A biochemical analysis linking APOBEC3A to disparate HIV-1 restriction and skin cancer, J. Biol. Chem. 288 (41) (2013) 29294–29304.
[8] R.S. Harris, Molecular mechanism and clinical impact of APOBEC3B-catalyzed mutagenesis in breast cancer, Breast Cancer Res. 17 (8) (2015).
[9] R.S. LaRue, V. Andresdottir, Y. Blanchard, S.G. Conticello, D. Derse, M. Emerman, W.C. Greene, S.R. Jonsson, N.R. Landau, M. Lochelt, H.S. Malik, M.H. Malim, C. Munk, S.J. O'Brien, V.K. Pathak, K. Strebel, S. Wain-Hobson, X.F. Yu, N. Yuhki, R.S. Harris, Guidelines for naming nonprimate APOBEC3 genes and proteins, J. Virol. 83 (2) (2009) 494–497.
[10] J.E. Wedekind, G.S. Dance, M.P. Sowden, H.C. Smith, Messenger RNA editing in mammals: new members of the APOBEC family seeking roles in the family business, Trends Genet. 19 (4) (2003) 207–216.
[11] S.G. Conticello, C.J. Thomas, S.K. Petersen-Mahrt, M.S. Neuberger, Evolution of the AID/APOBEC family of polynucleotide (deoxy)cytidine deaminases, Mol. Biol. Evol. 22 (2) (2005) 367–377.
[12] C. Barnes, H.C. Smith, Apolipoprotein B mRNA editing in vitro is a zinc-dependent process, Biochem. Biophys. Res. Commun. 197 (3) (1993) 5.
[13] L. Betts, S. Xiang, S.A. Short, R. Wolfenden, C.W. Carter Jr., Cytidine deaminase. The 2.3 a crystal structure of an enzyme: transition-state analog complex, J. Mol. Biol. 235 (2) (1994) 635–656.
[14] C.W. Carter, The nucleoside Deaminases for Cytidine and adenosine - structure, transition-state stabilization, mechanism, and evolution, Biochimie 77 (1–2) (1995) 92–98.
[15] H. Aydin, M.W. Taylor, J.E. Lee, Structure-guided analysis of the human APOBEC3-HIV restrictome, Structure 22 (5) (2014) 668–684.
[16] K.N. Bishop, R.K. Holmes, A.M. Sheehy, N.O. Davidson, S.J. Cho, M.H. Malim, Cytidine deamination of retroviral DNA by diverse APOBEC proteins, Curr. Biol. 14 (15) (2004) 1392–1396.
[17] M.T. Liddament, W.L. Brown, A.J. Schumacher, R.S. Harris, APOBEC3F properties and hypermutation preferences indicate activity against HIV-1 in vivo, Curr. Biol. 14 (15) (2004) 1385–1391.
[18] B.P. Doehle, A. Schafer, B.R. Cullen, Human APOBEC3B is a potent inhibitor of HIV-1 infectivity and is resistant to HIV-1 Vif, Virology 339 (2) (2005) 281–288.
[19] Y. Dang, X.J. Wang, W.J. Esselman, Y.H. Zheng, Identification of APOBEC3DE as another antiretroviral factor from the human APOBEC family, J. Virol. 80 (21) (2006) 10522–10533.
[20] F. Ito, Y. Fu, S.C.A. Kao, H.J. Yang, X.J.S. Chen, Family-wide comparative analysis of Cytidine and Methylcytidine deamination by eleven human APOBEC proteins, J. Mol. Biol. 429 (12) (2017) 1787–1799.
[21] Y.H. Zheng, D. Irwin, T. Kurosu, K. Tokunaga, T. Sata, B.M. Peterlin, Human APOBEC3F is another host factor that blocks human immunodeficiency virus type 1 replication, J. Virol. 78 (11) (2004) 6073–6076.
[22] C. Chaipan, J.L. Smith, W.S. Hu, V.K. Pathak, APOBEC3G restricts HIV-1 to a greater extent than APOBEC3F and APOBEC3DE in human primary CD4(+) T cells and macrophages, J. Virol. 87 (1) (2013) 444–453.
[23] A. Ara, R.P. Love, L. Chelico, Different mutagenic potential of HIV-1 restriction factors APOBEC3G and APOBEC3F is determined by distinct single-stranded DNA scanning mechanisms, PLoS Pathog. 10 (3) (2014).
[24] Y. Fang, X. Xiao, S.X. Li, A. Wolfe, X.S. Chen, Molecular interactions of a DNA modifying enzyme APOBEC3F catalytic domain with a single-stranded DNA, J. Mol. Biol. 430 (1) (2018) 87–101.
[25] W. Zennou, D. Perez-Caballero, H. Gottlinger, P.D. Bieniasz, APOBEC3G incorporation into human immunodeficiency virus type 1 particles, J. Virol. 78 (21) (2004) 12058–12061.
[26] C.S. Song, L. Sutton, M.E. Johnson, R.T. D'Aquila, J.P. Donahue, Signals in APOBEC3F N-terminal and C-terminal Deaminase domains each contribute to Encapsidation in HIV-1 Virions and are both required for HIV-1 restriction, J. Biol. Chem. 287 (20) (2012) 16965–16974.
[27] X. Wang, X.Y. Li, J. Ma, L. Zhang, L. Ma, Z.Y. Mi, J.M. Zhou, F. Guo, L. Kleiman, S. Cen, Human APOBEC3F incorporation into human immunodeficiency virus type 1 particles, Virus Res. 191 (2014) 30–38.
[28] B. Yang, K. Chen, C. Zhang, S. Huang, H. Zhang, Virion-associated uracil DNA glycosylase-2 and apurinic/apyrimidinic endonuclease are involved in the degradation of APOBEC3G-edited nascent HIV-1 DNA, J. Biol. Chem. 282 (16) (2007) 11667–11675.
[29] M. Marin, K.M. Rose, S.L. Kozak, D. Kabat, HIV-1 Vif protein binds the editing enzyme APOBEC3G and induces its degradation, Nat. Med. 9 (11) (2003) 1398–1403.
[30] S. Jager, D.Y. Kim, J.F. Hultquist, K. Shindo, R.S. LaRue, E. Kwon, M. Li, B.D. Anderson, L. Yen, D. Stanley, C. Mahon, J. Kane, K. Franks-Skiba, P. Cimermancic, A. Burlingame, A. Sali, C.S. Craik, R.S. Harris, J.D. Gross, N.J. Krogan, Vif hijacks CBF-beta to degrade APOBEC3G and promote HIV-1 infection, Nature 481 (7381) (2012) 371–375.
[31] K.D. Squires, M. Monajemi, C.F. Woodworth, M.D. Grant, M. Larijani, Impact of APOBEC mutations on CD8+ T cell recognition of HIV epitopes varies depending on the restricting HLA, J. Acquir. Immune Defic. Syndr. 70 (2) (2015) 172–178.
[32] M. Monajemi, C.F. Woodworth, K. Zipperlen, M. Gallant, M.D. Grant, M. Larijani, Positioning of APOBEC3G/F mutational hotspots in the human immunodeficiency virus genome favors reduced recognition by CD8+ T cells, PLoS ONE 9 (4) (2014) e93428.
[33] H.A. Sadler, M.D. Stenglein, R.S. Harris, L.M. Mansky, APOBEC3G contributes to HIV-1 variation through sublethal mutagenesis, J. Virol. 84 (14) (2010) 7396–7404.
[34] N. Wood, T. Bhattacharya, B.F. Keele, E. Giorgi, M. Liu, B. Gaschen, M. Daniels, G. Ferrari, B.F. Haynes, A. McMichael, G.M. Shaw, B.H. Hahn, B. Korber, C. Seoighe, HIV evolution in early infection: selection pressures, patterns of

insertion and deletion, and the impact of APOBEC, PLoS Pathog. 5 (5) (2009) e1000414.
[35] S. Venkatesan, R. Rosenthal, N. Kanu, N. McGranahan, J. Bartek, S.A. Quezada, J. Hare, R.S. Harris, C. Swanton, Perspective: APOBEC mutagenesis in drug resistance and immune escape in HIV and cancer evolution, Ann. Oncol. 29 (3) (2018) 563–572.
[36] M. Nakashima, H. Ode, T. Kawamura, S. Kitamura, Y. Naganawa, H. Awazu, S. Tsuzuki, K. Matsuoka, M. Nemoto, A. Hachiya, W. Sugiura, Y. Yokomaku, N. Watanabe, Y. Iwatani, Structural insights into HIV-1 Vif-APOBEC3F interaction, J. Virol. 90 (2) (2016) 1034–1047.
[37] C. Richards, J.S. Albin, O. Demir, N.M. Shaban, E.M. Luengas, A.M. Land, B.D. Anderson, J.R. Holten, J.S. Anderson, D.A. Harki, R.E. Amaro, R.S. Harris, The binding Interface between human APOBEC3F and HIV-1 Vif elucidated by genetic and computational approaches, Cell Rep. 13 (9) (2015) 1781–1788.
[38] K.K. Siu, A. Sultana, F.C. Azimi, J.E. Lee, Structural determinants of HIV-1 Vif susceptibility and DNA binding in APOBEC3F, Nat. Commun. 4 (2013).
[39] M.F. Bohn, S.M.D. Shandilya, J.S. Albin, T. Kouno, B.D. Anderson, R.M. McDougle, M.A. Carpenter, A. Rathore, L. Evans, A.N. Davis, J.Y. Zhang, Y.J. Lu, M. Somasundaran, H. Matsuo, R.S. Harris, C.A. Schiffer, Crystal structure of the DNA cytosine Deaminase APOBEC3F: the catalytically active and HIV-1 Vif-binding domain, Structure 21 (6) (2013) 1042–1050.
[40] L. Wan, T. Nagata, M. Katahira, Influence of the DNA sequence/length and pH on deaminase activity, as well as the roles of the amino acid residues around the catalytic center of APOBEC3F, Phys. Chem. Chem. Phys. 20 (5) (2018) 3109–3117.
[41] A. Furukawa, T. Nagata, A. Matsugami, Y. Habu, R. Sugiyama, F. Hayashi, N. Kobayashi, S. Yokoyama, H. Takaku, M. Katahira, Structure, interaction and real-time monitoring of the enzymatic reaction of wild-type APOBEC3G, EMBO J. 28 (4) (2009) 440–451.
[42] A. Furukawa, K. Sugase, R. Morishita, T. Nagata, T. Kodaki, A. Takaori-Kondo, A. Ryo, M. Katahira, Quantitative analysis of location- and sequence-dependent deamination by APOBEC3G using real-time NMR spectroscopy, Angew. Chem. Int. Ed. Eng. 53 (9) (2014) 2349–2352.
[43] K. Kamba, T. Nagata, M. Katahira, Catalytic analysis of APOBEC3G involving real-time NMR spectroscopy reveals nucleic acid determinants for deamination, PLoS ONE 10 (4) (2015) e0124142.
[44] K. Kamba, T. Nagata, M. Katahira, Characterization of the deamination coupled with sliding along DNA of anti-HIV factor APOBEC3G on the basis of the pH-dependence of deamination revealed by real-time NMR monitoring, Front. Microbiol. 7 (2016) 587.
[45] K. Kamba, T. Nagata, M. Katahira, The C-terminal cytidine deaminase domain of APOBEC3G itself undergoes intersegmental transfer for a target search, as revealed by real-time NMR monitoring, Phys. Chem. Chem. Phys. 20 (5) (2018) 2976–2981.
[46] L. Wan, T. Nagata, R. Morishita, A. Takaori-Kondo, M. Katahira, Observation by real-time NMR and interpretation of length- and location-dependent deamination activity of APOBEC3B, ACS Chem. Biol. 12 (11) (2017) 2704–2708.
[47] T. Goddard, D. Kneller, Sparky 3, University of California, San Francisco, 2006.
[48] D.C. Harris, Nonlinear least-squares curve fitting with Microsoft excel solver, J. Chem. Educ. 75 (1) (1998) 119–121.
[49] K. Shi, M.A. Carpenter, S. Banerjee, N.M. Shaban, K. Kurahashi, D.J. Salamango, J.L. McCann, G.J. Starrett, J.V. Duffy, O. Demir, R.E. Amaro, D.A. Harki, R.S. Harris, H. Aihara, Structural basis for targeted DNA cytosine deamination and mutagenesis by APOBEC3A and APOBEC3B, Nat. Struct. Mol. Biol. 24 (2) (2017) 131–139.
[50] S. Harjes, W.C. Solomon, M. Li, K.M. Chen, E. Harjes, R.S. Harris, H. Matsuo, Impact of H216 on the DNA binding and catalytic activities of the HIV restriction factor APOBEC3G, J. Virol. 87 (12) (2013) 7008–7014.
[51] T. Kouno, T.V. Silvas, B.J. Hilbert, S.M.D. Shandilya, M.F. Bohn, B.A. Kelch, W.E. Royer, M. Somasundaran, N. Kurt Yilmaz, H. Matsuo, C.A. Schiffer, Crystal structure of APOBEC3A bound to single-stranded DNA reveals structural basis for cytidine deamination and specificity, Nat. Commun. 8 (2017) 15024.
[52] A. Maiti, W. Myint, T. Kanai, K. Delviks-Frankenberry, C. Sierra Rodriguez, V.K. Pathak, C.A. Schiffer, H. Matsuo, Crystal structure of the catalytic domain of HIV-1 restriction factor APOBEC3G in complex with ssDNA, Nat. Commun. 9 (1) (2018) 2460.